Journal of Systems Engineering and Electronics
Vol. 26, No. 2, April 2015, pp.334–345

Modified super twisting controller for servicing to uncontrolled spacecraft

Binglong Chen and Yunhai Geng*

Research Center of Satellite Technology, Harbin Institute of Technology, Harbin 150080, China

Abstract: A relative position and attitude coupled sliding mode controller is proposed by combining the standard super twisting (ST) control and basic linear algorithm for autonomous rendezvous and docking. It is schemed for on-orbit servicing to a tumbling non-cooperative target spacecraft subjected to external disturbances. A coupled dynamic model is established including both kinematical and dynamic coupled effect of relative rotation on relative translation, which illustrates the relative movement between the docking port located in target spacecraft and another in service spacecraft. The modified super twisting (MST) control algorithm containing linear compensation items is schemed to manipulate the relative position and attitude synchronously. The correction provides more robustness and convergence velocity for dealing with linearly growing perturbations than the ST control algorithm. Moreover, the stability characteristic of closed-loop system is analyzed by Lyapunov method. Numerical simulations are adopted to verify the analysis with the comparison between MST and ST control algorithms. Simulation results demonstrate that the proposed MST controller is characterized by high precision, strong robustness and fast convergence velocity to attenuate the linearly increasing perturbations.

Keywords: autonomous rendezvous and docking, coupled dynamic model, modified super twisting, Lyapunov method.

DOI: 10.1109/JSEE.2015.00039

1. Introduction

The ability to perform routine autonomous rendezvous and docking (ARD) is needed in future space missions including assembly of international space station (ISS), autonomous deployment, manipulation and repair [1]. The collision probability increases with the decreasing distance between two spacecraft, especially docking with a tumbling non-cooperative target spacecraft [2,3]. Therefore, it is important to establish the full dynamics for ARD and controllers are designed to guarantee the reliability and success rate. Numbers of control strategies have been adopted for either orbital maneuvering or attitude tracking, such as adaptive control [4,5], optimal control [6,7] and sliding model control [8,9].

In prophase researches, models for relative translation and relative rotation are established separately, which restrict developments of its applications. Pan and Kapila [10] addressed a nonlinear tracking control problem with adaptive feedback control to deal with unknown mass and inertia matrix of spacecraft. They took into account the dynamic coupled effect caused by the gravity gradient torque on relative translation and the global asymptotical stability of tracking errors is proved by the Lyapunov framework. However, the relative translation model is on the basis of point-mass model and the controller is proposed for the open-loop system. Shay and Pini solved the errors resulted from the point-mass model in distributed spacecraft formation flying [11], and developed a kinematical coupled relative translation model between any arbitrary feature points on spacecraft. They consider the kinematical coupled effect of relative rotation on relative translation derived from relative angular velocity, but they neglect the kinematic coupled effect caused by absolute angular velocity of the leader spacecraft and another effect introduced by disturbances. Environmental disturbance torque is inevitable existence, and therefore we consider both kinematical and dynamical coupled effects of relative rotation on relative translation.

As is known to all, sliding mode control (SMC) is used widely because of the finite time convergence property and robustness for system uncertainties. Its capability to suppress disturbances is independent of dynamic model instead of modeling with uncertain states as the system function in robust control [12,13]. However, the standard SMC is based on 1-sliding mode [14] and it induces control chattering phenomenon caused by high frequency switching of control. Therefore, high order sliding mode (HOSM) technique is invented to eliminate the chattering phenomenon [15] by acting on the higher order time derivatives of the

Manuscript received April 02, 2014.
*Corresponding author.
This work was supported by the National Natural Science Foundation of China (61104026).

system deviation from the constraint. Consequently, there are increasing information demands in implementation of HOSM and the arbitrary order sliding mode control law is mostly still theoretically studied. However, 2-sliding mode (SOSM) algorithms, such as twisting and super twisting, have already been used successfully in real problems [16]. Super twisting sliding mode (ST) is one of widely used SOSM control algorithms [17,18], which can suppress bounded disturbances and does not need to use the derivative of the switching function. In contrast to the linear algorithm, the main disadvantage of SOSM algorithm is that it cannot endure the linearly growing perturbation. However, the linear algorithm is not able to support strong disturbance near the equilibrium point, which is one of advantages of the SOSM algorithm [19].

Inspired by the aforementioned issues, a modified super twisting sliding mode (MST) control algorithm is proposed by adding linear correction terms to the basic ST to obtain both excellent properties of them. It is applied in this study to design a relative position and attitude coupled SOSM controller. We take account of the bounded linearly increasing perturbations, the limited disturbance torques, model uncertainties and the actuator output saturation. The paper is organized as follows. In Section 2, a coupled dynamic model is established between the docking port located in target spacecraft with respect to another in service spacecraft including both kinematical and dynamic coupled effects of relative rotation on relative translation [20]. In Section 3, ST and MST are schemed to generate control operation of service spacecraft for making ARD with target spacecraft and the second method of Lyapunov is used to analyze the stability characteristic of the closed-loop system. In Section 4, numerical simulations are performed to verify the performance of MST by comparing with basic ST method for ARD without collision. Finally, the conclusions are represented in Section 5.

2. Coupled dynamic relative model

A coupled relative motion model is derived from the traditional point-mass model for relative motion between center-of-masses (CMs) of the target spacecraft and the service spacecraft. We take into consideration the kinematical coupled effect caused by relative attitude angular velocity, relative attitude quaternion and absolute attitude angular velocity of the service spacecraft and the dynamic coupled effect derived from external disturbance torques.

2.1 Coordinate systems

We define some coordinate systems to illustrate the relative motion between the two docking ports, so that the origins of coupled effects are distinct. The useful coordinate systems are shown in Fig. 1.

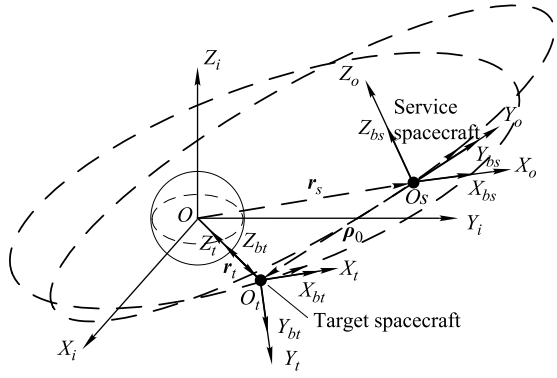

Fig. 1 Coordinate systems

The earth-centered inertial coordinate system ($\mathcal{F}_i$): $OX_iY_iZ_i$ is fixed in an inertial space. It is a right-handed system with the origin at the earth center O. X_i axis points the vernal equinox direction, Z_i axis is along the North Pole and Y_i axis completes the setup to yield a Cartesian right hand system.

Euler-Hill reference frame ($\mathcal{F}_o$): $O_sX_oY_oZ_o$ is fixed to the CM of the service spacecraft with the origin O_s. X_o axis is directing from the radially outward, Z_o axis is normal to the orbital plane, Y_o axis is pointing to the velocity direction of the service spacecraft in the orbital plane and perpendicular with O_sX_o. This frame is used to describe the attitude of the service spacecraft and the relative motion of the target spacecraft with respect to the service spacecraft.

Orbit coordinate system of the target spacecraft ($\mathcal{F}_t$): $O_tX_tY_tZ_t$ is fixed to the CM of the target spacecraft with the origin O_t. Z_t axis is pointing to the earth center O, Y_t axis is along the opposite direction of orbit angular rate and X_t is along the velocity direction of the target spacecraft completing a right hand system. This frame is used to describe the attitude of the target spacecraft.

Body coordinate system ($\mathcal{F}_b$): It is a Cartesian right-hand reference frame fixed on the spacecraft and originates at the spacecraft's CM. The body coordinate systems of the service spacecraft and the target spacecraft are denoted $\mathcal{F}_{bs}$ and $\mathcal{F}_{bt}$ respectively. It is assumed that $\mathcal{F}_{bs}$ and $\mathcal{F}_{bt}$ coincide with $\mathcal{F}_o$ and $\mathcal{F}_t$ separately at the initial time.

Therefore, euler angles and attitude angular velocities of the service spacecraft and the target spacecraft are defined respectively by relative rotational motion of $\mathcal{F}_b$ with respect to $\mathcal{F}_o$ and $\mathcal{F}_t$. Then definition of absolute attitude angular velocities, severally noted by $\boldsymbol{\omega}_{bs}$ and $\boldsymbol{\omega}_{bt}$, are rotational velocity of $\mathcal{F}_{bs}$ and $\mathcal{F}_{bt}$ relative to $\mathcal{F}_i$. Similarly, relative angular velocity ω_r is rotational velocity of $\mathcal{F}_{bt}$ with respect to $\mathcal{F}_{bs}$. Therefor, $\boldsymbol{\omega}_r$ can be expressed as

$$\boldsymbol{\omega}_r = \boldsymbol{\omega}_{bt} - \boldsymbol{\omega}_{bs}. \tag{1}$$

Then, the attitude can be parameterized by quaternion:

$$\boldsymbol{q} = [\boldsymbol{q}_v^{\mathrm{T}} \quad q_4]^{\mathrm{T}} \tag{2}$$

where $\boldsymbol{q}_v^{\mathrm{T}} = [q_1, q_2, q_3]$ is the vector part and q_4 is the scalar part. It is subjected to the constraint that $q_1^2 + q_2^2 + q_3^2 + q_4^2 = 1$. $\boldsymbol{q}_s$ and $\boldsymbol{q}_t$ are denotations for attitude of the service spacecraft and the target spacecraft. $\boldsymbol{q}_r$ denotes relative quaternion of $\mathcal{F}_{bt}$ with respect to $\mathcal{F}_{bs}$. Then, the rotation matrix can be expressed as

$$\boldsymbol{A}(\boldsymbol{q}) = (q_4^2 - \boldsymbol{q}_v^{\mathrm{T}}\boldsymbol{q}_v)\boldsymbol{I}_{3\times 3} + 2\boldsymbol{q}_v\boldsymbol{q}_v^{\mathrm{T}} - 2q_4\boldsymbol{q}_v^{\times} \tag{3}$$

where $[\cdot^{\times}]$ denotes the cross product matrix.

2.2 Relative rotation

Let $\boldsymbol{a}$ be an arbitrary vector measured with respect to the origin of $\mathcal{F}_i$ and $\dot{\boldsymbol{a}}|_{\mathcal{F}}$ denotes time derivative of $\boldsymbol{a}$ measured in the reference frame $\mathcal{F}$ and $(\boldsymbol{a})_{\mathcal{F}}$ is the expression in $\mathcal{F}$. According to (1), $\boldsymbol{\omega}_{bt}$ can be rewritten in $\mathcal{F}_{bt}$ as follows:

$$(\boldsymbol{\omega}_{bt})_{\mathcal{F}_{bt}} = (\boldsymbol{\omega}_r)_{\mathcal{F}_{bt}} + \boldsymbol{A}(\boldsymbol{q}_r)(\boldsymbol{\omega}_{bs})_{\mathcal{F}_{bs}}. \tag{4}$$

Due to the angular momentum theorem, the time derivative of (4) can be rewritten as

$$\begin{aligned}\dot{\boldsymbol{\omega}}_r\big|_{\mathcal{F}_{bt}} = \boldsymbol{J}_t^{-1}\{\boldsymbol{T}_t - [\boldsymbol{\omega}_r + \boldsymbol{A}(\boldsymbol{q}_r)\boldsymbol{\omega}_{bs}] \times \boldsymbol{J}_t \cdot \\ [\boldsymbol{\omega}_r + \boldsymbol{A}(\boldsymbol{q}_r)\boldsymbol{\omega}_{bs}]\} - \boldsymbol{A}(\boldsymbol{q}_r)\boldsymbol{J}_s^{-1}(\boldsymbol{T}_s - \boldsymbol{\omega}_{bs}\times \\ \boldsymbol{J}_s\boldsymbol{\omega}_{bs}) - [\boldsymbol{\omega}_r + \boldsymbol{A}(\boldsymbol{q}_r)\boldsymbol{\omega}_{bs}] \times (\boldsymbol{\omega}_r)_{\mathcal{F}_{bt}}\end{aligned} \tag{5}$$

where $\boldsymbol{J}$ is the inertia matrix and $\boldsymbol{T}$ consists of control torque $\boldsymbol{T}_c$, gravity gradient torque $\boldsymbol{T}_g$ and disturbance torque $\boldsymbol{T}_d$ as follows:

$$\begin{cases} \boldsymbol{T}_d = 1.5\times 10^{-5}\begin{bmatrix} 3\cos(\omega^{\circ}t) + 1 \\ 1.5\sin(\omega^{\circ}t) + 3\cos(\omega^{\circ}t) \\ 3\sin(\omega^{\circ}t) + 1 \end{bmatrix} \\ \boldsymbol{T}_g = 3\mu/r^3 \cdot \boldsymbol{Z}_0 \times \boldsymbol{J}\boldsymbol{Z}_0 \end{cases}$$

where ω° is the magnitude of the orbit angular velocity, μ is the earth gravitational constant, r is the magnitude of the radius vector from the CM of spacecraft to the earth's center and $\boldsymbol{Z}_0$ is the unit radius vector of r. Then, time derivative of the quaternion kinematical equation can be expressed as

$$\ddot{\boldsymbol{q}}_r = -0.25\boldsymbol{\omega}_r^{\mathrm{T}}\boldsymbol{\omega}_r\boldsymbol{q}_r + 0.5[\boldsymbol{Q}_v^{\mathrm{T}}, -\boldsymbol{q}_{rv}]^{\mathrm{T}}\dot{\boldsymbol{\omega}}_r \tag{6}$$

where

$$\boldsymbol{Q}_v = q_{r4}\boldsymbol{I}_{3\times 3} + \boldsymbol{q}_{rv}^{\times}. \tag{7}$$

Then the relative rotational model can be obtained by substituting (5) into (6). Express the vector part and it provides us with the following expression:

$$\ddot{\boldsymbol{q}}_{rv} = g(*) - 0.5\boldsymbol{Q}_v\boldsymbol{A}(\boldsymbol{q}_r)\boldsymbol{J}_s^{-1}\boldsymbol{T}_{sc} + \boldsymbol{\vartheta}_2 \tag{8}$$

where

$$\begin{aligned} g(*) = -0.25\boldsymbol{\omega}_r^{\mathrm{T}}\boldsymbol{\omega}_r\boldsymbol{q}_{rv} - 0.5\boldsymbol{Q}_v\boldsymbol{J}_t^{-1}[\boldsymbol{\omega}_r + \boldsymbol{A}(\boldsymbol{q}_r)\boldsymbol{\omega}_{bs}]\times \\ \boldsymbol{J}_t[\boldsymbol{\omega}_r + \boldsymbol{A}(\boldsymbol{q}_r)\boldsymbol{\omega}_{bs}] + 0.5\boldsymbol{Q}_v\boldsymbol{A}(\boldsymbol{q}_r)\boldsymbol{J}_s^{-1}(\boldsymbol{\omega}_{bs}\times\boldsymbol{J}_s\boldsymbol{\omega}_{bs}) - \\ 0.5\boldsymbol{Q}_v[(\boldsymbol{\omega}_r)_{\mathcal{F}_{bt}} + \boldsymbol{A}(\boldsymbol{q}_r)(\boldsymbol{\omega}_{bs})_{\mathcal{F}_{bs}}]\times(\boldsymbol{\omega}_r)_{\mathcal{F}_{bt}} \\ \boldsymbol{\vartheta}_2 = \frac{1}{2}\boldsymbol{Q}_v[\boldsymbol{J}_t^{-1}(\boldsymbol{T}_{tg} + \boldsymbol{T}_{td}) - \boldsymbol{A}(\boldsymbol{q}_r)\boldsymbol{J}_s^{-1}(\boldsymbol{T}_{sg} + \boldsymbol{T}_{sd})] \end{aligned}$$

and components of $\boldsymbol{\vartheta}_2$ can be limited by

$$\begin{aligned}|\vartheta_{2i}|_{\max} = 0.5\lambda_{\max}(\boldsymbol{Q}_v\boldsymbol{J}_t^{-1})\max(\boldsymbol{T}_{tg} + \boldsymbol{T}_{td}) + \\ 0.5\lambda_{\max}[\boldsymbol{Q}_v\boldsymbol{A}(\boldsymbol{q}_r)\boldsymbol{J}_s^{-1}]\max(\boldsymbol{T}_{sg} + \boldsymbol{T}_{sd})\end{aligned} \tag{9}$$

where $i = 1, 2, 3$; $\lambda_{\max}(\cdot)$ is the maximum eigenvalue of a matrix and $\max(\cdot)$ represents the maximum element of a vector.

2.3 Relative translation

Consider two docking ports located in the target spacecraft and the service spacecraft separately, as illustrated in Fig. 2. $\boldsymbol{P}_t^i$ denotes a vector directed from the origin of $\mathcal{F}_{bt}$ to the docking port P_t^i and $\boldsymbol{P}_s^j$ is directed from the origin of $\mathcal{F}_{bs}$ to the docking port P_s^j. By observing, we can obtain the relative position vector $\boldsymbol{\rho}_{ij}$ as

$$\boldsymbol{\rho}_{ij} = \boldsymbol{r}_t - \boldsymbol{r}_s + \boldsymbol{P}_t^i - \boldsymbol{P}_s^j \tag{10}$$

where $\boldsymbol{r}_t$, $\boldsymbol{r}_s$ are CM position vectors of the target spacecraft and the service spacecraft respectively. Then the second-order derivative of $\boldsymbol{\rho}_{ij}$ with respect to time in $\mathcal{F}_o$ can be calculated as

$$\begin{aligned}\ddot{\boldsymbol{\rho}}_{ij}\big|_{\mathcal{F}_o} = \mu/\boldsymbol{r}_s^3\boldsymbol{r}_s - \mu/\boldsymbol{r}_t^3\boldsymbol{r}_t - 2\boldsymbol{\omega}_s^{\circ}\times\dot{\boldsymbol{\rho}}_{ij}\big|_{\mathcal{F}_o} - \dot{\boldsymbol{\omega}}_s^{\circ}\big|_{\mathcal{F}_o}\times\boldsymbol{\rho}_{ij} - \\ \boldsymbol{\omega}_s^{\circ}\times(\boldsymbol{\omega}_s^{\circ}\times\boldsymbol{\rho}_{ij}) + \dot{\boldsymbol{\omega}}_{bt}\big|_{\mathcal{F}_{bt}}\times\boldsymbol{P}_t^i + \boldsymbol{\omega}_{bt}\times(\boldsymbol{\omega}_{bt}\times\boldsymbol{P}_t^i) - \\ \dot{\boldsymbol{\omega}}_{bs}\big|_{\mathcal{F}_{bs}}\times\boldsymbol{P}_s^j - \boldsymbol{\omega}_{bs}\times(\boldsymbol{\omega}_{bs}\times\boldsymbol{P}_s^j) - \boldsymbol{a}_{sc} + \boldsymbol{a}_{td} - \boldsymbol{a}_{sd}\end{aligned} \tag{11}$$

where $\boldsymbol{\omega}^{\circ}$ is the orbital angular velocity, $\boldsymbol{a}_{sc}$ is the control acceleration of the service spacecraft, $\boldsymbol{a}_{sd} = (1+k_dt)\boldsymbol{a}_{sd0}$, $\boldsymbol{a}_{td} = (1 + k_dt)\boldsymbol{a}_{td0}$ where k_d is the increasing rate.

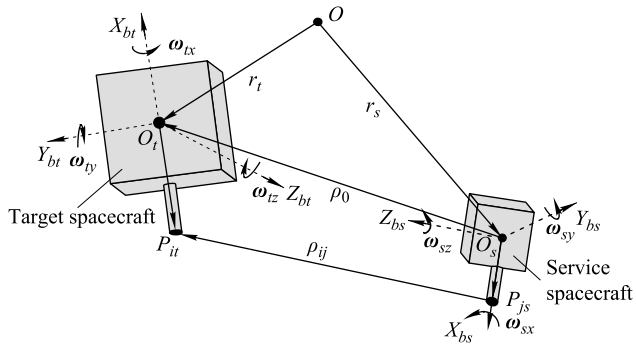

Fig. 2 Relative translation of docking ports

Moreover, the relative translational model can be expressed as

$$\ddot{\boldsymbol{\rho}}_{ij}\big|_{\mathcal{F}_o} = f(*) - \boldsymbol{G}\boldsymbol{T}_{sc} - \boldsymbol{A}^{\mathrm{T}}(\boldsymbol{q}_s)\boldsymbol{a}_{sc} + \boldsymbol{\vartheta}_1 \tag{12}$$

where

$$f(*) = \mu/\boldsymbol{r}_s^3\boldsymbol{r}_s - \mu/\boldsymbol{r}_t^3\boldsymbol{r}_t - 2\boldsymbol{\omega}_s^\circ \times \dot{\boldsymbol{\rho}}_{ij}\big|_{\mathcal{F}_o} - \dot{\boldsymbol{\omega}}_s^\circ\big|_{\mathcal{F}_o} \times \boldsymbol{\rho}_{ij} - \boldsymbol{\omega}_s^\circ \times (\boldsymbol{\omega}_s^\circ \times \boldsymbol{\rho}_{ij}) - \boldsymbol{A}^{\mathrm{T}}(\boldsymbol{q}_s)\boldsymbol{A}^{\mathrm{T}}(\boldsymbol{q}_r)\{\{\boldsymbol{J}_t^{-1}\cdot [\boldsymbol{\omega}_r + \boldsymbol{A}(\boldsymbol{q}_r)\boldsymbol{\omega}_{bs}] \times \boldsymbol{J}_t[\boldsymbol{\omega}_r + \boldsymbol{A}(\boldsymbol{q}_r)\boldsymbol{\omega}_{bs}]\} \times \boldsymbol{P}_t^i\} + \boldsymbol{A}^{\mathrm{T}}(\boldsymbol{q}_s)\{[\boldsymbol{A}^{\mathrm{T}}(\boldsymbol{q}_r)\boldsymbol{\omega}_r + \boldsymbol{\omega}_{bs}] \times \{[\boldsymbol{A}^{\mathrm{T}}(\boldsymbol{q}_r)\boldsymbol{\omega}_r + \boldsymbol{\omega}_{bs}] \times [\boldsymbol{A}^{\mathrm{T}}(\boldsymbol{q}_r)\boldsymbol{P}_t^i]\}\} + \boldsymbol{A}^{\mathrm{T}}(\boldsymbol{q}_s)\{[\boldsymbol{J}_s^{-1}(\boldsymbol{\omega}_{bs} \times \boldsymbol{J}_s\boldsymbol{\omega}_{bs})] \times \boldsymbol{P}_s^j\} - \boldsymbol{A}^{\mathrm{T}}(\boldsymbol{q}_s)[\boldsymbol{\omega}_{bs} \times (\boldsymbol{\omega}_{bs} \times \boldsymbol{P}_s^j)]$$

$$\boldsymbol{\vartheta}_1 = \boldsymbol{A}^{\mathrm{T}}(\boldsymbol{q}_s)\boldsymbol{A}^{\mathrm{T}}(\boldsymbol{q}_r)\{[\boldsymbol{J}_t^{-1}(\boldsymbol{T}_{tg} + \boldsymbol{T}_{td})] \times \boldsymbol{P}_t^i\} - \boldsymbol{A}^{\mathrm{T}}(\boldsymbol{q}_s)\{[\boldsymbol{J}_s^{-1}(\boldsymbol{T}_{sg} + \boldsymbol{T}_{sd})] \times \boldsymbol{P}_s^j\} - \boldsymbol{A}^{\mathrm{T}}(\boldsymbol{q}_s)\boldsymbol{a}_{sd} + \boldsymbol{A}^{\mathrm{T}}(\boldsymbol{q}_s)\boldsymbol{A}^{\mathrm{T}}(\boldsymbol{q}_r)\boldsymbol{a}_{td}$$

and $\boldsymbol{G}$ is determined by $\boldsymbol{J}_s$, $\boldsymbol{P}_s^j$ and $\boldsymbol{q}_s$. Then components of $\boldsymbol{\vartheta}_1$ can be limited as follows:

$$|\vartheta_{1i}|_{\max} = \max\{[\boldsymbol{J}_t^{-1}(\boldsymbol{T}_{tg} + \boldsymbol{T}_{td})] \times \boldsymbol{P}_t^i\} + \max\{[\boldsymbol{J}_s^{-1}(\boldsymbol{T}_{sg} + \boldsymbol{T}_{sd})] \times \boldsymbol{P}_s^j\} + \max(\boldsymbol{a}_{td0})(1 + k_d t) + \max(\boldsymbol{a}_{sd0})(1 + k_d t). \tag{13}$$

3. Control law design

Consider the state variable $\boldsymbol{x} = [\boldsymbol{\rho}_{ij}^{\mathrm{T}}, \boldsymbol{q}_{rv}^{\mathrm{T}}]^{\mathrm{T}}$, then the former relative position and attitude coupled dynamic model can be expressed as below by combining (8) and (12):

$$\ddot{\boldsymbol{x}} = \boldsymbol{sys}(*) - \begin{bmatrix} \boldsymbol{A}^{\mathrm{T}}(\boldsymbol{q}_s) & \boldsymbol{G} \\ \boldsymbol{0}_{3\times 3} & 0.5\boldsymbol{Q}_v\boldsymbol{A}(\boldsymbol{q}_r)\boldsymbol{J}_s^{-1} \end{bmatrix} \boldsymbol{u} + \boldsymbol{\vartheta} \tag{14}$$

where $\boldsymbol{\vartheta} = [\boldsymbol{\vartheta}_1^{\mathrm{T}}, \boldsymbol{\vartheta}_2^{\mathrm{T}}]^{\mathrm{T}}$, $\boldsymbol{sys}(*) = [f^{\mathrm{T}}(*), g^{\mathrm{T}}(*)]^{\mathrm{T}}$, $\boldsymbol{u} = [\boldsymbol{a}_{sc}^{\mathrm{T}}, \boldsymbol{T}_{sc}^{\mathrm{T}}]^{\mathrm{T}}$ and actuators outputs have saturation characteristic, which can be expressed as

$$\begin{cases} \text{if} \quad a_{sci} < a_{\max},\ (a_{sci})_{\mathrm{real}} = a_{sci} \\ \text{else}(a_{sci})_{\mathrm{real}} = a_{sci} \cdot a_{\max}/|a_{sci}| \\ \text{if} \quad T_{sci} < T_{\max},\ (T_{sci})_{\mathrm{real}} = T_{sci} \\ \text{else}(T_{sci})_{\mathrm{real}} = T_{sci} \cdot T_{\max}/|T_{sci}| \end{cases} \tag{15}$$

where $i = x, y, z$.

Let us define the desired control objective $\boldsymbol{x}_d = [\boldsymbol{\rho}_{ijd}^{\mathrm{T}}, \boldsymbol{q}_{rvd}^{\mathrm{T}}]^{\mathrm{T}}$, the state error $\boldsymbol{e} = \boldsymbol{x} - \boldsymbol{x}_d$ and $\dot{\boldsymbol{e}} = \dot{\boldsymbol{x}} - \dot{\boldsymbol{x}}_d$. The control goal is to enforce the sliding mode on the manifold $\boldsymbol{s} = \dot{\boldsymbol{e}} + \lambda\boldsymbol{e}$.

3.1 Standard ST design

According to the inequalities (9) and (13), we can suppose that the ith component of $\boldsymbol{\delta}$ is bounded by positive constants expressing as $|\delta_i| \leqslant \varepsilon_i|z_{1i}|^{1/2}$, where $\varepsilon_i = |\vartheta_{1i}|_{\max}$ $(i = 1, 2, 3)$ and $\varepsilon_j = |\vartheta_{2i}|_{\max}$ $(i = 1, 2, 3; j = i + 3)$. Thus, the ST controller is designed as follows:

$$\begin{cases} \boldsymbol{u} = [\boldsymbol{A}^{\mathrm{T}}(\boldsymbol{q}_s), \boldsymbol{G}; \boldsymbol{0}_{3\times 3}, 0.5\boldsymbol{Q}_v\boldsymbol{A}(\boldsymbol{q}_r)\boldsymbol{J}_s^{-1}]^{-1} \cdot \\ \qquad [\boldsymbol{sys}(*) + \boldsymbol{\lambda}\dot{\boldsymbol{e}} - \ddot{\boldsymbol{x}}_d + \boldsymbol{M}_1\mathrm{sign}(\boldsymbol{s})^{1/2} - \boldsymbol{z}_2] \\ \dot{\boldsymbol{z}}_2 = -\boldsymbol{M}_2\mathrm{sign}(\boldsymbol{s}) \end{cases} \tag{16}$$

where $\boldsymbol{M}_j$ $(j = 1, 2)$ is the main diagonal matrix with diagonal elements $M_{ji} > 0$. The function $\mathrm{sign}(\boldsymbol{s})^{1/2}$ is defined as follows:

$$\mathrm{sign}(\boldsymbol{s})^{1/2} = [|s_1|^{1/2}\mathrm{sign}(s_1), \ldots, |s_6|^{1/2}\mathrm{sign}(s_6)]^{\mathrm{T}} \tag{17}$$

and $\mathrm{sign}(\boldsymbol{s})$ is expressed as

$$\mathrm{sign}(\boldsymbol{s}) = [\mathrm{sign}(s_1), \ldots, \mathrm{sign}(s_6)]^{\mathrm{T}}.$$

Let $\boldsymbol{z} = [\boldsymbol{s}^{\mathrm{T}}, \boldsymbol{z}_2^{\mathrm{T}}]^{\mathrm{T}}$, the closed-loop system dynamics can be expressed as

$$\dot{\boldsymbol{z}} = \begin{bmatrix} -M_{1i}|s_i|^{1/2}\mathrm{sign}(s_i) + z_{2i} + \delta_i \\ -M_{2i}\mathrm{sign}(s_i) \end{bmatrix}.$$

Therefore, the system can converge to zero in finite time when the inequalities are satisfied.

$$M_{1i} > 2\varepsilon_i, \quad M_{2i} > \frac{(\varepsilon_i^2 + 8\varepsilon_i M_{1i})M_{1i}}{8(M_{1i} - 2\varepsilon_i)} \tag{18}$$

3.2 MST controller design

In this section, MST is designed based on standard ST algorithm and basic linear algorithm. These modification allows the control system to have both exponential and finite time convergence properties. According to the components of ϑ, it can be divided into two parts as follows:

$$\vartheta_i = \zeta_{1i} + \int_0^t \zeta_{2i}(\tau)\mathrm{d}\tau, \quad i = 1, 2, \ldots, 6$$

where

$$|\zeta_1|_{\max} = [\boldsymbol{J}_t^{-1}(|\boldsymbol{T}_{tg}|_{\max} + |\boldsymbol{T}_d|_{\max})] \times \boldsymbol{P}_t^i + \max(\boldsymbol{a}_{td0}) + [\boldsymbol{J}_s^{-1}(|\boldsymbol{T}_{sg}|_{\max} + |\boldsymbol{T}_d|_{\max})] \times \boldsymbol{P}_s^j + \max(\boldsymbol{a}_{sd0}) \cdot 0.5\lambda_{\max}(\boldsymbol{Q}_v\boldsymbol{J}_t^{-1})(|\boldsymbol{T}_{tg}|_{\max} + |\boldsymbol{T}_d|_{\max}) + 0.5\lambda_{\max}[\boldsymbol{Q}_v\boldsymbol{A}(\boldsymbol{q}_r)\boldsymbol{J}_s^{-1}](|\boldsymbol{T}_{sg}|_{\max} + |\boldsymbol{T}_d|_{\max})$$

$$|\zeta_2|_{\max} = \begin{bmatrix} k_d[\max(\boldsymbol{a}_{td0}) + \max(\boldsymbol{a}_{sd0})] \\ \boldsymbol{0}_{3\times 1} \end{bmatrix} \begin{cases} |\boldsymbol{T}_d|_{\max} = 1.5 \times 10^{-5} \begin{bmatrix} 4 \\ \sqrt{11.25} \\ 4 \end{bmatrix} \\ |\boldsymbol{T}_g|_{\max} = \dfrac{3\mu}{r^3}\max(\boldsymbol{Z}_0 \times \boldsymbol{J}\boldsymbol{Z}_0) \end{cases}$$

and they are assumed to be bounded by some positive constants δ_{ji} $(j=1,2,\ldots,4)$ as follows:

$$\begin{cases} |\zeta_{1i}| \leqslant \delta_{1i}|x_{1i}|^{1/2} + \delta_{3i}|x_{1i}| \\ |\zeta_{2i}| \leqslant \delta_{2i} + \delta_{4i}|x_{1i}| \end{cases} \tag{19}$$

where $\delta_{1i} = |\zeta_{1i}|_{\max}$, $\delta_{2i} = |\zeta_{2i}|_{\max}$, $\delta_{3i} > 0$, $\delta_{4i} > 0$; x_{1i} is the ith component of switching function $\boldsymbol{x}_1$ defined in the following section. The proposed MST controller is designed as follows:

$$\boldsymbol{u} = [\boldsymbol{A}^{\mathrm{T}}(\boldsymbol{q}_s), \boldsymbol{G}; \boldsymbol{0}_{3\times 3}, 0.5\boldsymbol{Q}_v\boldsymbol{A}(\boldsymbol{q}_r)\boldsymbol{J}_s^{-1}]^{-1}\cdot$$

$$[\boldsymbol{sys}(*) + \lambda\dot{\boldsymbol{e}} - \ddot{\boldsymbol{x}}_d + \boldsymbol{K}_1\mathrm{sign}(\boldsymbol{s})^{1/2} + \boldsymbol{K}_2\boldsymbol{s} - \boldsymbol{Z}] \tag{20}$$

where

$$\dot{\boldsymbol{Z}} = -\boldsymbol{K}_3\mathrm{sign}(\boldsymbol{s}) - \boldsymbol{K}_4\boldsymbol{s}$$

and $\boldsymbol{K}_j$ $(j=1,\ldots,4)$ is the main diagonal matrix with $k_{ji} > 0$ as the diagonal elements.

Let us define vector $\boldsymbol{x} = [\boldsymbol{x}_1, \boldsymbol{x}_2]$ where $\boldsymbol{x}_1 = \boldsymbol{s}$, $\boldsymbol{x}_2 = \boldsymbol{Z} + \int_0^t \zeta_2(\tau)\mathrm{d}\tau$. Thus the dynamic functions of the closed-loop system can be expressed as

$$\begin{cases} \dot{x}_{1i} = -k_{1i}|x_{1i}|^{1/2}\mathrm{sign}(x_{1i}) - k_{2i}x_{1i} + x_{2i} + \zeta_{1i} \\ \dot{x}_{2i} = -k_{3i}\mathrm{sign}(x_{1i}) - k_{4i}x_{1i} + \zeta_{2i} \end{cases}. \tag{21}$$

In what follows, the proof of finite time convergence to equilibrium point in MST law is given by the second method of Lyapunov.

3.3 MST stability analysis

The Lyapunov function for system (21) is defined with perturbations as follows:

$$V_i = 2k_{3i}|x_{1i}| + k_{4i}x_{1i}^2 + 0.5x_{2i}^2 +$$

$$0.5(k_{1i}|x_{1i}|^{1/2}\mathrm{sign}(x_{1i}) + k_{2i}x_{1i} - x_{2i})^2 = \boldsymbol{\xi}^{\mathrm{T}}\boldsymbol{P}\boldsymbol{\xi} > 0 \tag{22}$$

where

$$\begin{cases} \boldsymbol{\xi}^{\mathrm{T}} = [|x_{1i}|^{1/2}\mathrm{sign}(x_{1i}), x_{1i}, x_{2i}] \\ \boldsymbol{P} = \dfrac{1}{2}\begin{bmatrix} 4k_{3i} + k_{1i}^2 & k_{1i}k_{2i} & -k_{1i} \\ k_{1i}k_{2i} & 2k_{4i} + k_{2i}^2 & -k_{2i} \\ -k_{1i} & -k_{2i} & 2 \end{bmatrix} \end{cases}.$$

Note that V_i is continuous but it is not differentiable at $x_{1i} = 0$ and it is positive definite and radially unbounded if $k_{ji} > 0$.

$$\begin{cases} \lambda_{\min}(\boldsymbol{P})\|\boldsymbol{\xi}\|^2 \leqslant V_i \leqslant \lambda_{\max}(\boldsymbol{P})\|\boldsymbol{\xi}\|^2 \\ \|\boldsymbol{\xi}\|^2 = |x_{1i}| + x_{1i}^2 + x_{2i}^2 \end{cases} \tag{23}$$

where $\lambda_{\min}(\boldsymbol{P})$ and $\lambda_{\max}(\boldsymbol{P})$ denote the minimum and maximum eigenvalues of the matrix $\boldsymbol{P}$. Then the derivative of V_i with respect to time can be expressed as

$$\dot{V}_i = -|x_{1i}|^{-1/2}\boldsymbol{\xi}^{\mathrm{T}}\boldsymbol{\Omega}_{1i}\boldsymbol{\xi} - \boldsymbol{\xi}^{\mathrm{T}}\boldsymbol{\Omega}_{2i}\boldsymbol{\xi} + \boldsymbol{\omega}_{1i}^{\mathrm{T}}\boldsymbol{\xi} + |x_{1i}|^{-1/2}\boldsymbol{\omega}_{2i}^{\mathrm{T}}\boldsymbol{\xi} \tag{24}$$

$$\boldsymbol{\omega}_{1i}^{\mathrm{T}} = [k_{1i}(1.5k_{2i}\zeta_{1i} - \zeta_{2i}), (2k_{4i} + k_{2i}^2)\zeta_{1i} - k_{2i}\zeta_{2i}, -k_{2i}\zeta_{1i} + 2\zeta_{2i}]$$

$$\boldsymbol{\omega}_{2i}^{\mathrm{T}} = \zeta_{1i}[2k_{3i} + 0.5k_{1i}^2, 0, -0.5k_{1i}]$$

$$\boldsymbol{\Omega}_{1i} = k_{1i}/2\begin{bmatrix} 2k_{3i} + k_{1i}^2 & 0 & -k_{1i} \\ 0 & 2k_{4i} + 5k_{2i}^2 & -3k_{2i} \\ -k_{1i} & -3k_{2i} & 1 \end{bmatrix}$$

$$\boldsymbol{\Omega}_{2i} = k_{2i}\begin{bmatrix} k_{3i} + 2k_{1i}^2 & 0 & 0 \\ 0 & k_{4i} + k_{2i}^2 & -k_{2i} \\ 0 & -k_{2i} & 1 \end{bmatrix}.$$

$$\boldsymbol{\omega}_{1i}^{\mathrm{T}}\boldsymbol{\xi} + |x_{1i}|^{-1/2}\boldsymbol{\omega}_{2i}^{\mathrm{T}}\boldsymbol{\xi} \leqslant [3/2k_{1i}k_{2i}|x_{1i}|^{1/2} + (2k_{4i} + k_{2i}^2)\cdot |x_{1i}| + (2k_{3i} + k_{1i}^2/2) + (k_{2i} + k_{1i}/2|x_{1i}|^{-1/2})\mathrm{sign}(x_{1i})\cdot x_{2i}](\delta_{1i}|x_{1i}|^{1/2} + \delta_{3i}|x_{1i}|) + [k_{1i}|x_{1i}|^{1/2} + k_{2i}|x_{1i}| + 2\mathrm{sign}(x_{1i})x_{2i}](\delta_{2i} + \delta_{4i}|x_{1i}|) = |x_{1i}|^{-1/2}\boldsymbol{\xi}^{\mathrm{T}}\boldsymbol{\Delta}_{1i}\boldsymbol{\xi} + \boldsymbol{\xi}^{\mathrm{T}}\boldsymbol{\Delta}_{2i}\boldsymbol{\xi}$$

can be established if $x_{1i}x_{2i} > 0$, where

$$\begin{cases} \boldsymbol{\Delta}_{1i} = \begin{bmatrix} \delta_{2i}k_{1i} + 2\delta_{1i}k_{3i} + \dfrac{1}{2}\delta_{1i}k_{1i}^2 & 0 & \delta_{2i} + \dfrac{1}{4}\delta_{1i}k_{1i} \\ 0 & 0 & 0 \\ \delta_{2i} + \dfrac{1}{4}\delta_{1i}k_{1i} & 0 & 0 \end{bmatrix} \\ \boldsymbol{\Delta}_{2i} = \begin{bmatrix} \dfrac{1}{2}\delta_{3i}k_{1i}^2 + \dfrac{3}{2}\delta_{1i}k_{1i}k_{2i} + \delta_{2i}k_{2i} + 2\delta_{3i}k_{3i} & \dfrac{1}{2}\delta_{4i}k_{1i} + \delta_{1i}k_{4i} + \dfrac{3}{4}\delta_{3i}k_{1i}k_{2i} + \dfrac{1}{2}\delta_{1i}k_{2i}^2 & \dfrac{1}{4}\delta_{3i}k_{1i} + \dfrac{1}{2}\delta_{1i}k_{2i} \\ \dfrac{1}{2}\delta_{4i}k_{1i} + \delta_{1i}k_{4i} + \dfrac{3}{4}\delta_{3i}k_{1i}k_{2i} + \dfrac{1}{2}\delta_{1i}k_{2i}^2 & \delta_{3i}k_{2i}^2 + \delta_{4i}k_{2i} + 2\delta_{3i}k_{4i} & \delta_{4i} + \dfrac{1}{2}\delta_{3i}k_{2i} \\ \dfrac{1}{4}\delta_{3i}k_{1i} + \dfrac{1}{2}\delta_{1i}k_{2i} & \delta_{4i} + \dfrac{1}{2}\delta_{3i}k_{2i} & 0 \end{bmatrix} \end{cases}.$$

Thus, (24) can be rewritten as $\dot{V}_i \leqslant -|x_{1i}|^{-1/2}\boldsymbol{\xi}^{\mathrm{T}}\boldsymbol{Q}_{1i}\boldsymbol{\xi} - \boldsymbol{\xi}^{\mathrm{T}}\boldsymbol{Q}_{2i}\boldsymbol{\xi}(\boldsymbol{Q}_{1i} = \boldsymbol{\Omega}_{1i} - \boldsymbol{\Delta}_{1i}, \boldsymbol{Q}_{2i} = \boldsymbol{\Omega}_{2i} - \boldsymbol{\Delta}_{2i})$. If $x_{1i}x_{2i} < 0$,

$$\boldsymbol{\omega}_{1i}^{\mathrm{T}}\boldsymbol{\xi} + |x_{1i}|^{-1/2}\boldsymbol{\omega}_{2i}^{\mathrm{T}}\boldsymbol{\xi} \leqslant$$

$$\left[\frac{3}{2}k_{1i}k_{2i}|x_{1i}|^{1/2} + (2k_{4i} + k_{2i}^2)|x_{1i}| + \left(2k_{3i} + \frac{k_{1i}^2}{2}\right) - \left(k_{2i} + \frac{k_{1i}}{2}|x_{1i}|^{-1/2}\right)\mathrm{sign}(x_{1i})x_{2i}\right] \times$$

$$(\delta_{1i}|x_{1i}|^{1/2} + \delta_{3i}|x_{1i}|) + [k_{1i}|x_{1i}|^{1/2} + k_{2i}|x_{1i}| - 2\mathrm{sign}(x_{1i})x_{2i}](\delta_{2i} + \delta_{4i}|x_{1i}|) =$$

$$|x_{1i}|^{-1/2}\boldsymbol{\xi}^{\mathrm{T}}\boldsymbol{\Delta}_{3i}\boldsymbol{\xi} + \boldsymbol{\xi}^{\mathrm{T}}\boldsymbol{\Delta}_{4i}\boldsymbol{\xi}$$

where

$$\begin{cases} \boldsymbol{\Delta}_{3i} = \begin{bmatrix} \delta_{2i}k_{1i} + 2\delta_{1i}k_{3i} + \frac{1}{2}\delta_{1i}k_{1i}^2 & 0 & -\delta_{2i} - \frac{1}{4}\delta_{1i}k_{1i} \\ 0 & 0 & 0 \\ -\delta_{2i} - \frac{1}{4}\delta_{1i}k_{1i} & 0 & 0 \end{bmatrix} \\ \boldsymbol{\Delta}_{4i} = \begin{bmatrix} \frac{1}{2}\delta_{3i}k_{1i}^2 + \frac{3}{2}\delta_{1i}k_{1i}k_{2i} + \delta_{2i}k_{2i} + 2\delta_{3i}k_{3i} & \frac{1}{2}\delta_{4i}k_{1i} + \delta_{1i}k_{4i} + \frac{3}{4}\delta_{3i}k_{1i}k_{2i} + \frac{1}{2}\delta_{1i}k_{2i}^2 & -\frac{1}{4}\delta_{3i}k_{1i} - \frac{1}{2}\delta_{1i}k_{2i} \\ \frac{1}{2}\delta_{4i}k_{1i} + \delta_{1i}k_{4i} + \frac{3}{4}\delta_{3i}k_{1i}k_{2i} + \frac{1}{2}\delta_{1i}k_{2i}^2 & \delta_{3i}k_{2i}^2 + \delta_{4i}k_{2i} + 2\delta_{3i}k_{4i} & -\delta_{4i} - \frac{1}{2}\delta_{3i}k_{2i} \\ -\frac{1}{4}\delta_{3i}k_{1i} - \frac{1}{2}\delta_{1i}k_{2i} & -\delta_{4i} - \frac{1}{2}\delta_{3i}k_{2i} & 0 \end{bmatrix} \end{cases}.$$

Then (24) can be rewritten as

$$\dot{V}_i \leqslant -|x_{1i}|^{-1/2}\boldsymbol{\xi}^{\mathrm{T}}\boldsymbol{Q}_{3i}\boldsymbol{\xi} - \boldsymbol{\xi}^{\mathrm{T}}\boldsymbol{Q}_{4i}\boldsymbol{\xi}$$

$$(\boldsymbol{Q}_{3i} = \boldsymbol{\Omega}_{3i} - \boldsymbol{\Delta}_{3i}, \boldsymbol{Q}_{4i} = \boldsymbol{\Omega}_{4i} - \boldsymbol{\Delta}_{4i}).$$

Thus, we can derive $\dot{V} < 0$ if k_{ji} are appropriately chosen to make the matrices $\boldsymbol{Q}_{ji}$ be positive definite. Under this condition, system (22) is the global asymptotic stability and has finite time convergence property. When $\boldsymbol{Q}_{1i}$ is positive definite, the every sequential principal minor of $\boldsymbol{Q}_{1i}$ has a positive determinant. It can be represented by the formula as follows:

$$\begin{cases} k_{1i}k_{3i} + 0.5k_{1i}^3 - \delta_{2i}k_{1i} - 2\delta_{1i}k_{3i} - 0.5\delta_{1i}k_{1i}^2 > 0 \\ (k_{1i}k_{3i} + 0.5k_{1i}^3 - \delta_{2i}k_{1i} - 2\delta_{1i}k_{3i} - 0.5\delta_{1i}k_{1i}^2)\cdot \\ \quad (k_{1i}k_{4i} + 2.5k_{1i}k_{2i}^2) > 0 \\ |\boldsymbol{Q}_{1i}| > 0 \end{cases} \tag{25}$$

Thus we can get the following solutions

$$\begin{cases} k_{1i} > 2\max(\delta_{1i}, \sqrt{\delta_{2i}}) \\ k_{3i} > [36k_{1i}^4k_{2i}^2 + 4\delta_{1i}k_{1i}^3k_{2i}^2 + 16\delta_{1i}k_{1i}^3k_{4i} + (5\delta_{1i}^2 + 48\delta_{2i})k_{1i}^2k_{2i}^2 + (2\delta_{1i}^2 + 48\delta_{2i})k_{1i}^2k_{4i} + \\ \quad 40\delta_{2i}(\delta_{1i}k_{1i} + 2\delta_{2i})k_{2i}^2 + 16\delta_{2i}(\delta_{1i}k_{1i} + 2\delta_{2i})k_{4i}]/16k_{1i}(k_{1i} - 2\delta_{1i})(k_{4i} - 2k_{2i}^2) \\ k_{4i} > 2k_{2i}^2 \end{cases}. \tag{26}$$

It is noted that the first and second order principal minor determinants of $\boldsymbol{Q}_{3i}$ are the same as $\boldsymbol{Q}_{1i}$'s. Thus we only need to guarantee the determinant of $\boldsymbol{Q}_{3i}$ is positive. It is noticeable that $|\boldsymbol{Q}_{3i}| > 0$ can be consequentially satisfied as long as $|\boldsymbol{Q}_{1i}| > 0$.

Next, we calculate the conditions to make sure that $\boldsymbol{Q}_{2i}$ is positive definite. By using the same method mentioned above, we get the following conditions

$$\begin{cases} k_{2i}k_{3i} + 2k_{1i}^2k_{2i} - 0.5\delta_{3i}k_{1i}^2 - \\ \quad 1.5\delta_{1i}k_{1i}k_{2i} - \delta_{2i}k_{2i} - 2\delta_{3i}k_{3i} > 0 \\ (k_{2i}k_{3i} + 2k_{1i}^2k_{2i} - 0.5\delta_{3i}k_{1i}^2 - 1.5\delta_{1i}k_{1i}k_{2i} - \\ \quad \delta_{2i}k_{2i} - 2\delta_{3i}k_{3i})(k_{2i}k_{4i} + k_{2i}^3 - \delta_{3i}k_{2i}^2 - \\ \quad \delta_{4i}k_{2i} - 2\delta_{3i}k_{4i}) > (0.5\delta_{4i}k_{1i} + \delta_{1i}k_{4i} + \\ \quad 0.75\delta_{3i}k_{1i}k_{2i} + 0.5\delta_{1i}k_{2i}^2)^2 \\ |\boldsymbol{Q}_{2i}| > 0 \end{cases} \tag{27}$$

Therefore, the solutions can be expressed as

$$k_{1i} \leqslant \frac{\delta_{1i}(15\delta_{3i}^2 + 2\delta_{4i}) + \sqrt{\delta_{1i}^2(15\delta_{3i}^2 + 2\delta_{4i})^2 + \delta_{2i}(10\delta_{3i}^2 + \delta_{4i})\mathcal{D}}}{\mathcal{D}/4} \tag{28}$$

where

$$\mathcal{D} = (50 + 4\sqrt{69})\delta_{4i} - 31\delta_{3i}^2 > 0$$

$$\mathcal{M}_i = 4k_{2i}^2k_{3i}/k_{1i}^2 + 61/4k_{2i}^2 + 1.5\delta_{4i} + 4\delta_{1i}\delta_{4i}/k_{1i}$$

$$\mathcal{N}_i = 7k_{2i}^4 + (10\delta_{1i}\delta_{3i}/k_{1i} + 24\delta_{2i}\delta_{3i}/k_{1i}^2)k_{2i}^3 + k_{2i}^2k_{3i}(47\delta_{3i}^2 - 12\delta_{4i})/k_{1i}^2 + [(22\delta_{3i}^2 - 109\delta_{4i})/4 + (14\delta_{1i}\delta_{4i} + 2.5\delta_{1i}\delta_{3i}^2)/k_{1i} + (12\delta_{2i}\delta_{4i} + \delta_{2i}\delta_{3i}^2)/k_{1i}^2]\cdot k_{2i}^2 + 2(10\delta_{3i}\delta_{4i} + \delta_{3i}^3)k_{2i}k_{3i}/k_{1i}^2 + (\delta_{3i}^3 + 2\delta_{1i}\delta_{3i}\delta_{4i}/k_{1i} +$$

$$4\delta_{2i}\delta_{3i}\delta_{4i}/k_{1i}^2)k_{2i}+\{[8\delta_{3i}^2\delta_{4i}-4(k_{2i}^4+\delta_{4i}^2)]/k_{1i}^2+8\delta_{3i}\delta_{4i}^2/k_{1i}^2k_{2i}\}k_{3i}+\delta_{3i}^2\delta_{4i}/4-9\delta_{4i}^2+4\delta_{1i}\delta_{4i}^2/k_{1i}+\delta_{3i}\delta_{4i}^2/k_{2i}+4\delta_{2i}\delta_{4i}^2/k_{1i}^2>0$$

$$\mathcal{P}_i=\left(31+120\delta_{1i}/k_{1i}+160\delta_{2i}/k_{1i}^2\right)\delta_{3i}^2+16\left(\delta_{1i}/k_{1i}+\delta_{2i}/k_{1i}^2\right)\delta_{4i}$$

$$\mathcal{Q}_i=32k_{4i}^2+25\delta_{4i}k_{4i}+4\delta_{4i}^2$$

$$\mathcal{R}_i=2\left(31+120\delta_{1i}/k_{1i}+160\delta_{2i}/k_{1i}^2\right)\delta_{3i}^2-\left[100-32\left(\delta_{1i}/k_{1i}+\delta_{2i}/k_{1i}^2\right)\right]\delta_{4i}$$

Finally, we note that the first and second order principal minor determinants of $\boldsymbol{Q}_{4i}$ are the same as $\boldsymbol{Q}_{2i}$. Then we need only to guarantee $|\boldsymbol{Q}_{4i}|>0$ is satisfied. By the same method above, we get

$$2k_{2i}^2<k_{4i}<\left(-\mathcal{A}_i+\sqrt{\mathcal{A}_i^2+4\mathcal{B}_i}\right)/2,\ \mathcal{B}_i>0 \quad (29)$$

$$\begin{cases}\mathcal{A}_i=8k_{2i}^2k_{3i}/k_{1i}^2+53k_{2i}^2/4+1.5\delta_{4i}\\ \mathcal{B}_i=61k_{2i}^4/4+(14\delta_{1i}\delta_{3i}/k_{1i}+16\delta_{2i}\delta_{3i}/k_{1i}^2)k_{2i}^3+\\ \quad(32\delta_{3i}^2-2\delta_{4i})k_{2i}^2k_{3i}/k_{1i}^2+[(7.5+2.5\delta_{1i}/k_{1i}+\\ \quad\delta_{2i}/k_{1i}^2)\delta_{3i}^2-25\delta_{4i}/4]k_{2i}^2+2\delta_{3i}^3k_{2i}k_{3i}/k_{1i}^2+\\ \quad(\delta_{3i}^3+2\delta_{1i}\delta_{3i}\delta_{4i}/k_{1i}+4\delta_{2i}\delta_{3i}\delta_{4i}/k_{1i}^2)k_{2i}+\\ \quad[(8\delta_{3i}^2\delta_{4i}+7.75k_{2i}^4-4\delta_{4i}^2)/k_{1i}^2+\\ \quad8\delta_{3i}\delta_{4i}^2/k_{1i}^2k_{2i}]k_{3i}+\delta_{3i}^2\delta_{4i}/4-9\delta_{4i}^2+\\ \quad4\delta_{1i}\delta_{4i}^2/k_{1i}+\delta_{3i}\delta_{4i}^2/k_{2i}+4\delta_{2i}\delta_{4i}^2/k_{1i}^2\end{cases}$$

As mentioned above, the matrices $\boldsymbol{Q}_{ji}$ $(j=1,\dots,4;i=1,\dots,6)$ are positive definite when (26), (28) and (29) are satisfied. Thus the origin $\boldsymbol{x}=\boldsymbol{0}_{12\times1}$ is an equilibrium point that is strongly globally asymptotically stable.

According to (23), we can obtain

$$\|\boldsymbol{\xi}\|_{\max}=V_i^{1/2}/\lambda_{\min}^{1/2}(\boldsymbol{P})\geqslant\|\boldsymbol{\xi}\|\geqslant V_i^{1/2}/\lambda_{\max}^{1/2}(\boldsymbol{P})=\|\boldsymbol{\xi}\|_{\min}$$

$$\|\boldsymbol{\xi}\|\geqslant|x_{1i}|^{1/2},\|\boldsymbol{\xi}\|\geqslant\|\boldsymbol{\xi}\|_{\min}^2/\|\boldsymbol{\xi}\|_{\max}$$

and

$$\begin{cases}\|\boldsymbol{\xi}\|^2\geqslant|x_{1i}|^{1/2}\lambda_{\min}^{1/2}(\boldsymbol{P})/\lambda_{\max}(\boldsymbol{P})\cdot V_i^{1/2}\\ \|\boldsymbol{\xi}\|^2\geqslant1/\lambda_{\max}(\boldsymbol{P})\cdot V_i\end{cases},$$

so

$$\boldsymbol{\xi}^{\mathrm{T}}\boldsymbol{Q}_{ji}\boldsymbol{\xi}\geqslant\lambda_{\min}(\boldsymbol{Q}_{ji})\|\boldsymbol{\xi}\|^2 \quad (30)$$

where $\lambda_{\min}(\boldsymbol{Q}_{ji})$ is represented as the minimum eigenvalue of $\boldsymbol{Q}_{ji}$. Consequently, derivative of V_i with respect to time can be rewritten as

$$\dot{V}_i\leqslant-\gamma_{1i}V_i^{1/2}-\gamma_{2i}V_i \quad (31)$$

where

$$\begin{cases}\gamma_{1i}=\min[\lambda_{\min}(\boldsymbol{Q}_{1i}),\lambda_{\min}(\boldsymbol{Q}_{3i})]\lambda_{\min}^{1/2}(\boldsymbol{P})/\lambda_{\max}(\boldsymbol{P})\\ \gamma_{2i}=\min[\lambda_{\min}(\boldsymbol{Q}_{2i}),\lambda_{\min}(\boldsymbol{Q}_{4i})]/\lambda_{\max}(\boldsymbol{P})\end{cases}.$$

Since the solution of differential equation

$$\dot{V}_i=-\gamma_{1i}V_i^{1/2}-\gamma_{2i}V_i,V_i(0)=V_{i0},V(T_{fi})=0 \quad (32)$$

is given as follows:

$$\begin{cases}V_i(t)=\mathrm{e}^{-\gamma_{2i}\cdot t}[V_i(t_0)^{1/2}+\gamma_{1i}/\gamma_{2i}\cdot(1-\mathrm{e}^{\gamma_{2i}\cdot t/2})]\\ T_{fi}=2/\gamma_{2i}\cdot\ln(1+\gamma_{2i}/\gamma_{1i}\cdot V_{i0}^{1/2})\end{cases} \quad (33)$$

Thus we can obtain that V_i converges to zero in finite time and reaches zero at most after $\max(T_{fi})$ units of time.

4. Simulation results

4.1 Parameters initialization

The classical orbit elements of the target spacecraft and the service spacecraft are listed in Table 1. $\boldsymbol{\omega}_{tb}$ ($\boldsymbol{\omega}_{sb}$) denotes the angular velocity of $\mathcal{F}_{bt}$ ($\mathcal{F}_{bs}$) with respect to $\mathcal{F}_t$ ($\mathcal{F}_o$). The initialization values of them are separately $\boldsymbol{\omega}_{sb0}=\boldsymbol{0}_{3\times1}$ (°)/s and $\boldsymbol{\omega}_{tb0}=[-3.0\ \ 2.0\ \ 3.0]$ (°)/s. The mass characteristics are in Table 2. The numerical simulations are performed with linearly increasing disturbance accelerations of $\boldsymbol{a}_{td}=(1+k_dt)[2.5\ \ 4.0\ \ 3.8]^{\mathrm{T}}\times10^{-5}$ m/s^2 and $\boldsymbol{a}_{sd}=(1+k_dt)[2.0\ \ 4.2\ \ 3.8]^{\mathrm{T}}\times10^{-5}$ m/s^2.

Table 1 Classical orbit elements

Parameter	Value	
Semi-major/km	a_t= 7 170.0	a_s= 7 170.0
Eccentricity	e_t= 0.050 0	e_s= 0.050 0
Inclination/(°)	i_t=15.000 2	i_s=15.000 0
Ascending node/(°)	Ω_t=30.000 1	Ω_s=30.000 0
Argument of perigee/(°)	ω_t=10.000 0	ω_s=10.000 0
True anomaly/(°)	θ_t=20.000 2	θ_s=20.000 0

Table 2 Mass characteristics of the service spacecraft and the target spacecraft

Property	Values
$\boldsymbol{J}_s$/(kgm^2)	diag([45.6, 47.3, 46.9])
$\boldsymbol{J}_t$/(kgm^2)	diag([67.6, 57.6, 57.6])
m_s/kg	240
m_t/kg	320

The docking port vectors on the service spacecraft and the target spacecraft are expressed in respective body coordinate systems as follows:

$$\begin{cases}(\boldsymbol{P}_s^0)_{\mathcal{F}_{bs}}=[0.5,0.0,0.0]^{\mathrm{T}}\mathrm{m}\\ (\boldsymbol{P}_t^0)_{\mathcal{F}_{bt}}=[-0.75,0.0,0.0]^{\mathrm{T}}\mathrm{m}\end{cases}.$$

The control parameters of standard ST and MST algorithms are designed separately

$$\begin{cases}\boldsymbol{\lambda}=\mathrm{diag}([0.5,0.5,0.5,0.5,0.5,0.5])\\ \boldsymbol{M}_1=\mathrm{diag}([0.465,0.45,0.45,0.054,0.054,0.054])\\ \boldsymbol{M}_2=\mathrm{diag}([80.0,100.0,100.0,0.75,0.6,0.6])\times10^{-5}\\ \boldsymbol{K}_1=\mathrm{diag}([0.45,0.45,0.45,0.053,0.042,0.042])\\ \boldsymbol{K}_2=\mathrm{diag}([1.0,1.0,1.0,0.1,2.0,2.0])\times10^{-5}\\ \boldsymbol{K}_3=\mathrm{diag}([8.0,10.0,10.0,0.4,0.2,0.2])\times10^{-4}\\ \boldsymbol{K}_4=\mathrm{diag}([1.0,1.0,1.0,0.1,2.0,2.0])\times10^{-9}\end{cases}.$$

Bipropellant orbit and attitude control engines are chosen to operate relative position and attitude maneuvers synchronously. Output limitations of orbit and attitude control engines are $a_{\max} = 0.2$ m/s^2 and $T_{\max} = 0.8$ N·m. The control object is $\boldsymbol{x}_d = \dot{\boldsymbol{x}}_d = \boldsymbol{0}_{6\times1}$. In simulations, measurements of relative position, relative velocity and relative attitude angular velocity are assumed to be given by state estimator and so measure errors are ignored.

4.2 Results

When $k_d = 0$, the relative translation of docking port P_t^0 with respect to P_s^0 is shown in Fig. 3. Through comparing the two sliding mode control methods, illustrations show that the convergence time is approximate 30 s in MST while the standard ST needs more than 35 s to converge. The relative translational control accuracy of the two controllers are both calculated with data from 65 s to 100 s. The control accuracies are expressed as errors in 3σ (σ is the standard deviation). The relative position errors and relative velocity errors are listed in Table 3. As a result, the relative position errors are less than 2.4×10^{-6} m (3σ) and relative velocity errors are less than 5.4×10^{-4} m/s (3σ) in MST technique. By contrast, we can easily conclude that the MST algorithm has almost the same control effects without disturbances but MST has faster convergence time than ST method.

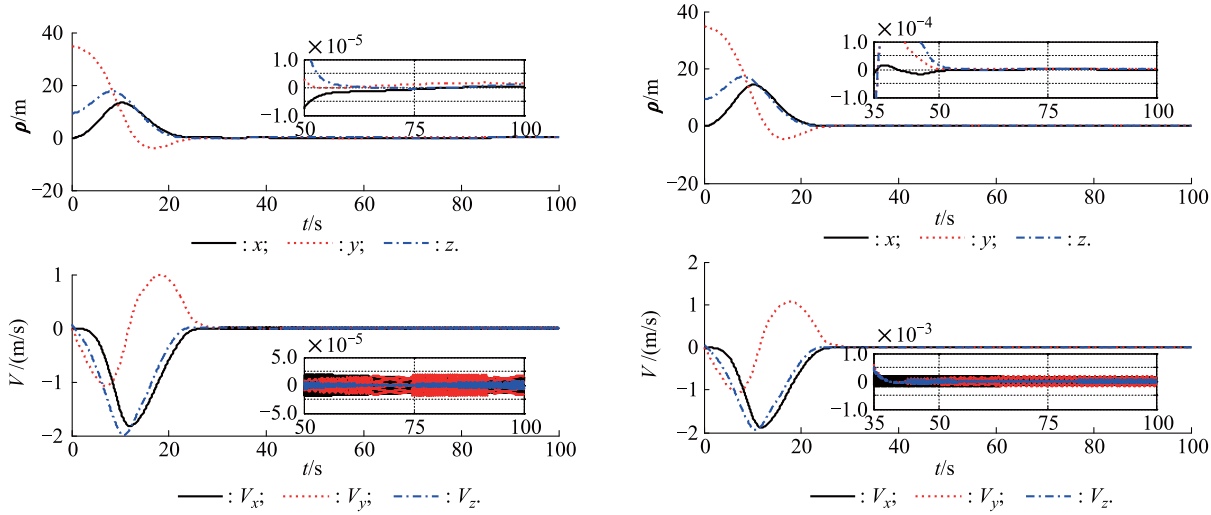

Fig. 3 Relative translation of docking ports in $\mathcal{F}_{bs}$

Table 3 Relative translation errors in 3σ

Parameter	Control errors	
	MST	ST
ΔX/m	1.240×10^{-6}	0.744×10^{-6}
ΔY/m	2.388×10^{-6}	2.080×10^{-6}
ΔZ/m	1.538×10^{-6}	2.639×10^{-6}
ΔV_x/(m/s)	3.940×10^{-4}	4.073×10^{-4}
ΔV_y/(m/s)	5.340×10^{-4}	5.410×10^{-4}
ΔV_z/(m/s)	1.190×10^{-4}	1.313×10^{-4}

Meanwhile, the relative rotation of the target spacecraft with respect to the service spacecraft are shown in Fig. 4. The control errors of relative attitude angles and relative angular velocity are listed in Table 4 by the same method as previously. Thus the relative attitude angle errors are less than 4.6×10^{-6} (°) (3σ) and relative angular velocity errors are less than 5.1×10^{-4} (°)/s (3σ) in MST algorithm. It is shown clearly again that the control accuracies of MST are higher than ST.

The relative distance between CMs of the service spacecraft and the target spacecraft and that of the two docking ports are illustrated in Fig. 5 by designed MST and ST algorithms respectively. The symbol $|\boldsymbol{\rho}_{ij}|$ indicates relative distance of docking port P_t^0 relative to P_s^0 and distance between permanent CMs of the target spacecraft and the service spacecraft is denoted by $|\boldsymbol{\rho}_{00}|$. The control errors of relative distance between the two docking ports are 2.038×10^{-6} m (3σ) by MST method and 2.098×10^{-6} m (3σ) in ST controller. It shows visibly that the MST controller has distinct advantages in terms of less convergence time and higher control precision than the basic ST algorithm.

Table 4 Relative rotation errors in 3σ

Parameter	Magnitude	
	MST	ST
$\Delta\phi_r$/(°)	-0.603×10^{-6}	6.447×10^{-6}
$\Delta\theta_r$/(°)	4.451×10^{-6}	5.902×10^{-6}
$\Delta\psi_r$/(°)	-1.569×10^{-6}	-1.065×10^{-6}
$\Delta\omega_x$/((°)/s)	6.162×10^{-4}	6.442×10^{-4}
$\Delta\omega_y$/((°)/s)	3.861×10^{-4}	6.409×10^{-4}
$\Delta\omega_z$/((°)/s)	3.907×10^{-4}	6.422×10^{-4}

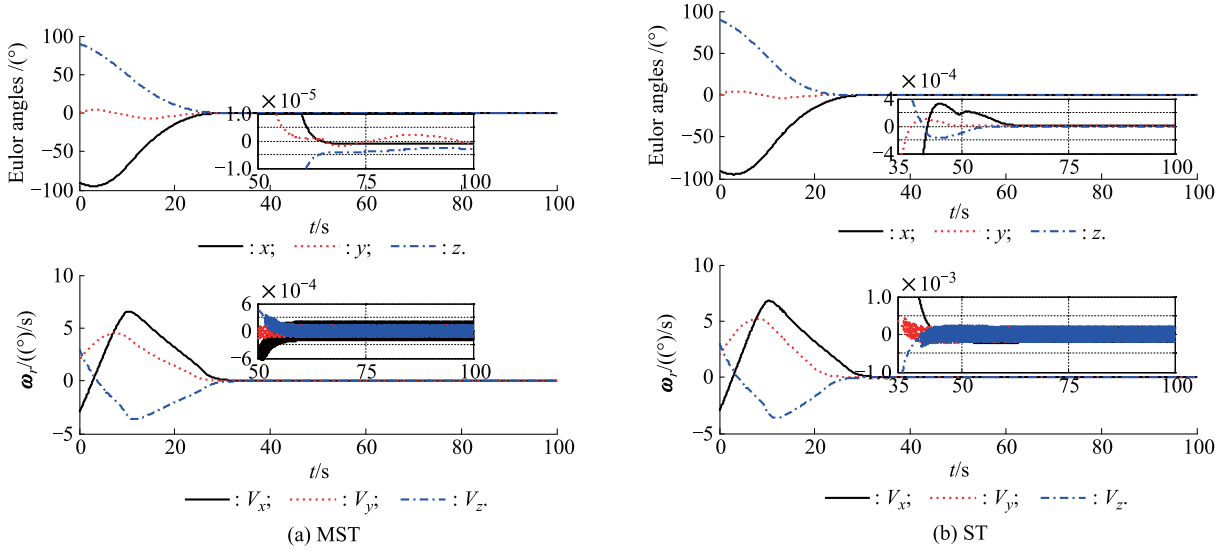

Fig. 4 Relative rotation of T with respect to the service spacecraft

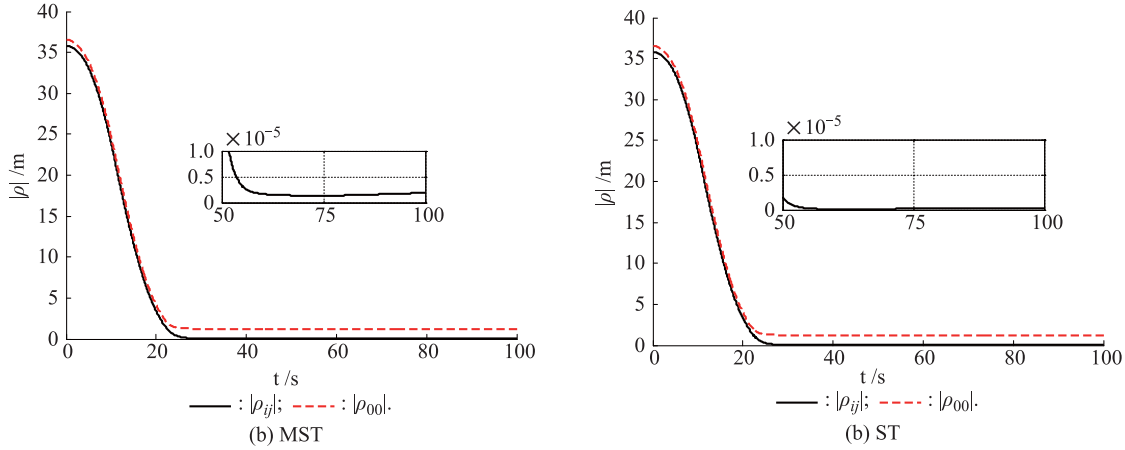

Fig. 5 Relative distance of docking ports

Furthermore, the control forces and torques outputted by the orbit and attitude control engines with saturation limits in MST and ST are illustrated in Fig. 6. Meanwhile, the sliding surfaces are described in Fig. 7, where S_x, S_y and S_z are relative position sliding surface components; S_{q1}, S_{q2} and S_{q3} are vector components of the relative quaternion. They present obviously again that the convergence time with MST algorithm is less than that used in ST method.

In order to verify the robustness of MST for linearly increasing disturbances, we increase k_d several times and the control accuracies of relative translation are listed in Table 5 by comparison with ST controller in the same other simulation conditions and the same precision calculation method. Simulation results indicate obviously that the proposed MST algorithm has stronger robustness for linearly increasing perturbations than ST method and the previous analytic analysis can be proofed accordingly.

Then we increase the inertia matrix by $\pm 15\%$ to verify the robustness of MST for modeling uncertainty and inertial matrix parameters uncertainties. Emulation programs are performed again with $k_d = 1.0$ and the same other parameters as before and the control accuracies are shown in Table 6. The results show that the proximity operation can be performed with almost the same magnitude of precision as the previous simulation. The analysis of control accuracy can be obtained as follows. The precision of relative position is 3.983×10^{-6} m (3σ), relative velocity accuracy is 5.354×10^{-4} m/s (3σ) and control error of relative distance between two docking ports is 4.088×10^{-6} m (3σ). Moreover, the accuracy of relative attitude angle is 9.790×10^{-6} (°) (3σ) and the relative angular velocity error is less than 8.6×10^{-4} (°)/s (3σ). As a consequence, the strong robustness and high reliability of MST are demonstrated, which can guaranty the ARD process is collisions-free.

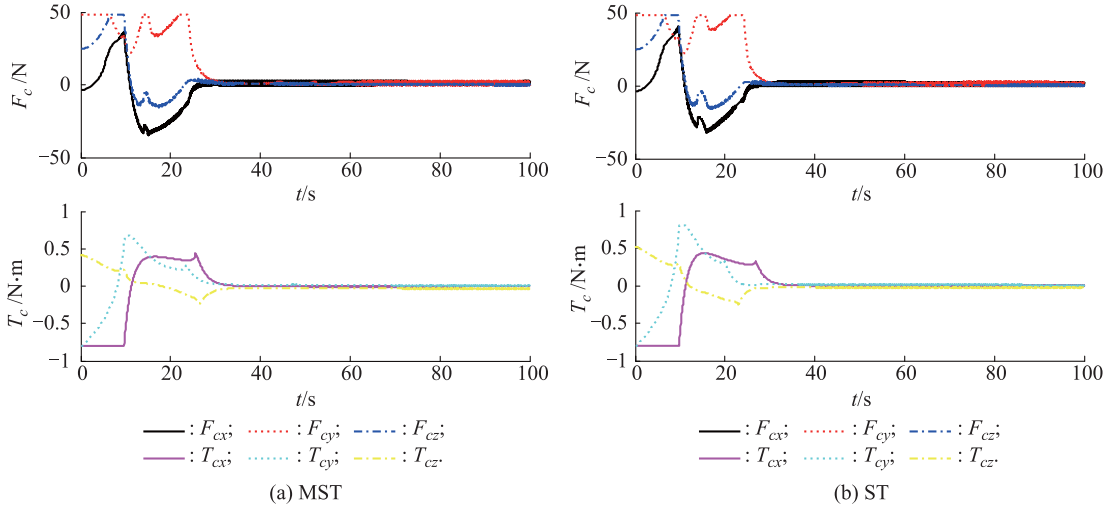

(a) MST (b) ST

Fig. 6 Actuators outputs in $\mathcal{F}_{bs}$

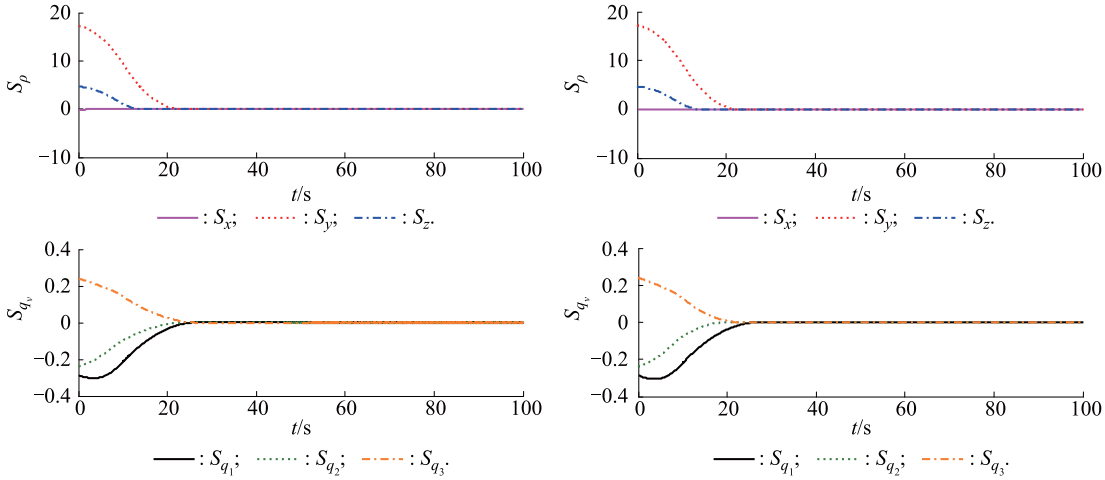

(a) MST (b) ST

Fig. 7 Sliding surfaces

Table 5 Control precisions in 3σ of relative translation under linearly increasing disturbances

Parameter	$k_d = 1.0$		$k_d = 3.0$	
	MST	ST	MST	ST
ΔX/m	3.380×10^{-6}	3.567×10^{-6}	4.090×10^{-6}	4.701×10^{-6}
ΔY/m	3.832×10^{-6}	4.183×10^{-6}	4.120×10^{-6}	4.413×10^{-6}
ΔZ/m	2.430×10^{-6}	3.249×10^{-6}	0.946×10^{-6}	1.809×10^{-6}
ΔV_x/(m/s)	3.940×10^{-4}	4.073×10^{-4}	3.937×10^{-4}	4.073×10^{-4}
ΔV_y/(m/s)	5.341×10^{-4}	5.411×10^{-4}	5.346×10^{-4}	5.412×10^{-4}
ΔV_z/(m/s)	1.188×10^{-4}	1.310×10^{-4}	1.188×10^{-4}	1.310×10^{-4}
$\Delta\lvert\boldsymbol{\rho}_{ij}\rvert$/m	3.770×10^{-6}	4.268×10^{-6}	4.189×10^{-6}	4.418×10^{-6}
Parameter	$k_d = 4.0$		$k_d = 5.0$	
	MST	ST	MST	ST
ΔX/m	4.288×10^{-6}	4.710×10^{-6}	4.827×10^{-6}	5.140×10^{-6}
ΔY/m	4.660×10^{-6}	4.832×10^{-6}	4.635×10^{-6}	4.851×10^{-6}
ΔZ/m	1.176×10^{-6}	1.907×10^{-6}	1.414×10^{-6}	1.355×10^{-6}
ΔV_x/(m/s)	3.942×10^{-4}	4.070×10^{-4}	3.938×10^{-4}	4.070×10^{-4}
ΔV_y/(m/s)	5.342×10^{-4}	5.417×10^{-4}	5.348×10^{-4}	5.418×10^{-4}
ΔV_z/(m/s)	1.187×10^{-4}	1.311×10^{-4}	1.188×10^{-4}	1.311×10^{-4}
$\Delta\lvert\boldsymbol{\rho}_{ij}\rvert$/m	4.673×10^{-6}	4.883×10^{-6}	4.930×10^{-6}	5.037×10^{-6}

Table 6 Control accuracy with model uncertainties in 3σ

Parameters	Increasement magnitudes of S and T			
	$+15\%, -15\%$	$+15\%, +15\%$	$-15\%, +15\%$	$-15\%, -15\%$
ΔX/m	3.376×10^{-6}	3.365×10^{-6}	3.524×10^{-6}	3.502×10^{-6}
ΔY/m	3.931×10^{-6}	3.908×10^{-6}	3.983×10^{-6}	3.970×10^{-6}
ΔZ/m	2.797×10^{-6}	2.795×10^{-6}	1.927×10^{-6}	1.952×10^{-6}
ΔV_x/(m/s)	3.934×10^{-4}	3.937×10^{-4}	3.941×10^{-4}	3.938×10^{-4}
ΔV_y/(m/s)	5.354×10^{-4}	5.353×10^{-4}	5.326×10^{-4}	5.327×10^{-4}
ΔV_z/(m/s)	1.183×10^{-4}	1.181×10^{-4}	1.200×10^{-4}	1.202×10^{-4}
$\Delta \phi_r$/(°)	5.363×10^{-6}	4.961×10^{-6}	8.223×10^{-6}	9.790×10^{-6}
$\Delta \theta_r$/(°)	-0.037×10^{-6}	-0.098×10^{-6}	0.928×10^{-6}	0.878×10^{-6}
$\Delta \psi_r$/(°)	3.494×10^{-6}	3.294×10^{-6}	2.535×10^{-6}	3.212×10^{-6}
$\Delta \omega_x$/((°)/s)	4.647×10^{-4}	4.655×10^{-4}	8.595×10^{-4}	8.595×10^{-4}
$\Delta \omega_y$/((°)/s)	2.919×10^{-4}	2.919×10^{-4}	5.390×10^{-4}	5.391×10^{-4}
$\Delta \omega_z$/((°)/s)	2.943×10^{-4}	2.943×10^{-4}	5.389×10^{-4}	5.389×10^{-4}
$\Delta \lvert \boldsymbol{\rho}_{ij} \rvert$/m	4.088×10^{-6}	4.070×10^{-6}	3.958×10^{-6}	3.983×10^{-6}

5. Conclusions

In this paper, a coupled relative motion model was established for the docking port located in target spacecraft and another in service spacecraft with the coupled effects of relative rotation on relative translation. The considered coupling effects belong to both kinematical and dynamic coupled effects. On the basis of this dynamic model, a modified super twisting sliding mode controller with linear correction terms was proposed to operate the relative position and attitude synchronously for on-orbit servicing to a tumbling non-cooperative target spacecraft subjected to some disturbances. Furthermore, by using the second method of Lyapunov, the finite time convergence property of the closed-loop system was proved. Numerical simulations were presented to validate the previous analysis by contrast with the standard super twisting algorithm. Simulation results illustrated that the revised super twisting controller has higher control precision, stronger robustness and faster convergence velocity for linearly increasing perturbations and mode uncertainties than the basic one.

References

[1] A. Flores-Abad, O. Ma, K. Pham, et al. A review of space robotics technologies for on-orbit servicing. *Progress in Aerospace Sciences*, 2014, 68: 1 – 26.

[2] K. Miller, J. Masciarelli, R. Rohrschneider. Advances in multi-mission autonomous rendezvous and docking and relative navigation capabilities. *Proc. of the IEEE Aerospace Conference*, 2012: 1 – 9.

[3] S. D'Amico, J. S. Ardaens, G. Gaias, et al. Noncooperative rendezvous using angles-only optical navigation: system design and flight results. *Journal of Guidance, Control, and Dynamics*, 2013, 36(6): 1576 – 1595.

[4] V. I. Utkin, A. S. Poznyak. Adaptive sliding mode control with application to super-twist algorithm: equivalent control method. *Automatica*, 2013, 49(1): 39 – 47.

[5] X. G. Dong, X. B. Cao, J. X. Zhang, et al. A robust adaptive control law for satellite formation flying. *Acta Automatica Sinica*, 2013, 39(2): 132 – 141.

[6] D. W. Gao, J. J. Luo, W. H. Ma, et al. Nonlinear optimal control of spacecraft approaching and tracking a non-cooperative maneuvering object. *Journal of Astronautics*, 2013, 34(6): 773 – 781.

[7] X. Y. Gao, K. L. Teo, G. R. Duan. An optimal control approach to robust control of nonlinear spacecraft rendezvous system with θ-D technique. *International Journal Innovative Computing, Information and Control*, 2013, 9(5): 2099 – 2110.

[8] C. Pukdeboon. Finite-time second-order sliding mode controllers for spacecraft attitude tracking. *Mathematical Problems in Engineering*, 2013, Article ID 930269.

[9] S. Janardhanan, M. Un Nabi, P. M. Tiwari. Attitude control of magnetic actuated spacecraft using super-twisting algorithm with nonlinear sliding surface. *Proc. of the 12th International Workshop on Variable Structure Systems*, 2012: 46 – 51.

[10] H. Z. Pan, V. Kapila. Adaptive nonlinear control for spacecraft formation flying with coupled translational and attitude dynamics. *Proc. of the IEEE Conference on Decision and Control*, 2001: 2057 – 2062.

[11] S. Shay, G. Pini. Effect of kinematic rotation-translation coupling on relative spacecraft translational dynamics. *Journal of Guidance, Control, and Dynamics*, 2009, 32(3): 1045 – 1050.

[12] A. Capua, A. Shapiro, D. Choukroun. Robust nonlinear H_∞ output-feedback for spacecraft attitude control. *Proc. of the AIAA Guidance, Navigation, and Control Conference – SciTech Forum and Exposition*, 2014: AIAA – 0455.

[13] A. M. Zou, K. D. Kumar. Robust attitude coordination control for spacecraft formation flying under actuator failures. *Journal of Guidance, Control, and Dynamics*, 2012, 35(4): 1247 – 1255.

[14] A. Levant. Sliding order and sliding accuracy in sliding mode control. *International Journal of Control*, 1993, 58(6): 1247 – 1263.

[15] W. Perruquetti, J. P. Barbot. *Sliding mode control in engineering*. New York: Marcel Dekker, 2002.

[16] A. Levant. Principles of 2-sliding mode design. *Automatica*, 2007, 43(4): 576 – 586.

[17] V. I. Utkin. About second order sliding mode control, relative degree, finite-time convergence and disturbance rejection. *Proc. of the 11th International Workshop on Variable Structure Systems*, 2010: 528 – 533.

[18] C. Pukdeboon. Second-order sliding mode controllers for spacecraft relative translation. *Applied Mathematical Sciences*, 2012, 6(100): 4965 – 4979.

[19] J. A. Moreno, M. Osorio. A Lyapunov approach to second-order sliding mode controllers and observers. *Proc. of the 47th IEEE Conference on Decision and Control*, 2008: 2856 – 2861.

[20] B. L. Chen, Y. H. Geng. Relative motion coupled dynamic modeling between two docking ports. *Systems Engineering and Electronics*, 2014, 36(4): 714 – 720. (in Chinese)

Biographies

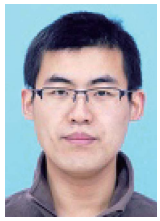

Binglong Chen was born in 1984. He received his B.E. and M.E. degrees in the School of Astronautics, Harbin Institute of Technology, in 2008 and 2010, respectively. He is now a Ph. D. student in the Research Center of Satellite Technology, Harbin Institute of Technology. His research interests are spacecraft navigation and spacecraft attitude and orbit control methods.
E-mail: chenbinglonghit@163.com

Yunhai Geng was born in 1970. He received his B.E. degree in engineering mechanics from Tongji University, M.E. and Ph.D. degrees in spacecraft design from Harbin Institute of Technology, in 1992, 1995 and 2003 respectively. Currently, he is a professor and doctoral advisor of spacecraft design, Harbin Institute of Technology. He has published about 60 journal and conference papers. His research interests include spacecraft attitude and orbit control, and spacecraft dynamics navigation guidance and control technology.
E-mail: gengyh@hit.edu.cn